CHAPTER 4

Testing the experimental absorber

4.1 Introduction

This chapter will document all the methods used for characterising the experimental vibration absorber. It will also report the most important experimental results.

The properties of the elastomeric spring are of extreme importance, since they are difficult to calculate during the design and have a big influence on the value of the isolation frequency. The first part of the chapter will therefore address techniques for the measurement of the stiffness and the loss factor. The first few methods used constant frequency excitation. From the data, the relaxation of the spring could be calculated. The second method employed sine sweep excitation. This method gave the properties as a function of frequency. Lastly, the transmissibility was calculated. From these measurements, the system properties could be extracted.

Two separate tests were done with the experimental absorber. The first test was with a 55 Shore A spring and the second with a 35 Shore A spring. The second spring was fitted to reduce the stiffness and thereby the isolation frequency.

A schematic of the test set-up is shown in figure 4.1. The load cells were used to measure the transmissibility. The LVDT and the top load cell were used to calculate the spring stiffness and loss factor. The actuator was set in displacement control for all tests to ensure that the specimen is not subjected to large displacements that could damage the spring.

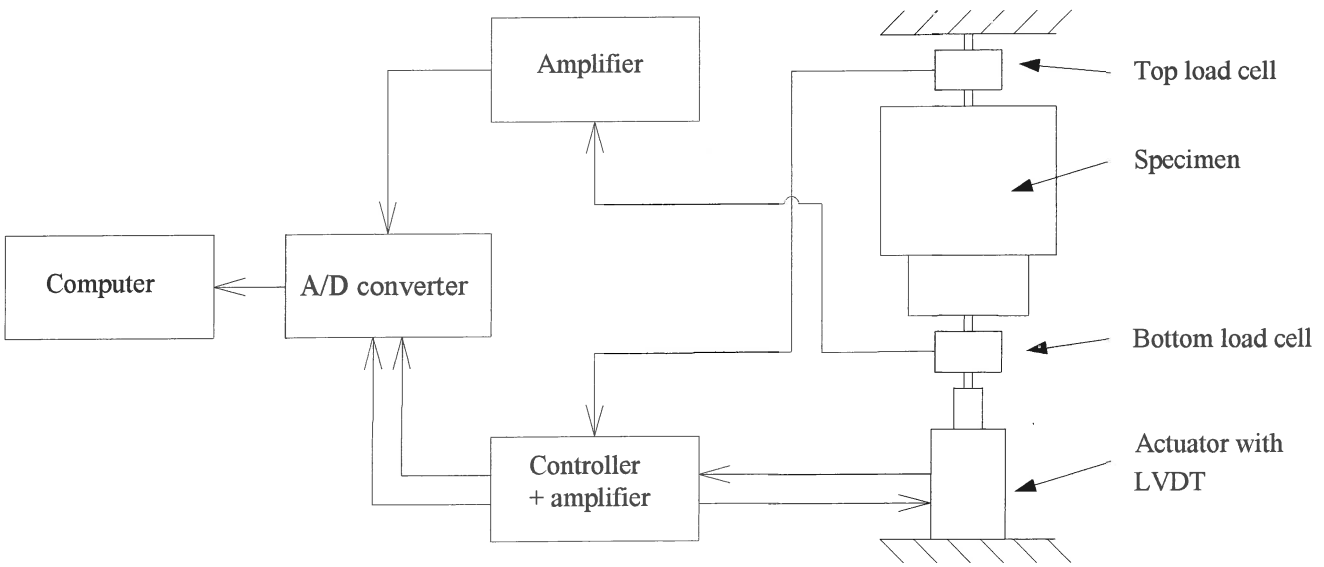

Figure 4.1 Schematic of the test set-up

The hydraulic actuator's controller was also used to amplify the signal from the top load cell and the LVDT. A second amplifier was needed for the bottom load cell. A CDAS analogue to digital converter was used to digitise the signal. The CDAS filter was set well above the excitation frequency. A Pentium computer with QanTIM software was used to generate the sine sweep signals. The constant frequency excitation signals were generated by the Schenk controller.

4.2 Constant frequency excitation

Constant frequency excitation was used to study how the properties of the elastomeric spring changed as a function of time. Data was gathered at 1-minute intervals, each for 1 second at a sampling frequency of 500 Hz. The total time of excitation was at least 1½ hours. These tests were done at 5 Hz intervals from 5 to 40 Hz.

The stiffness and loss factor will be reported. Three methods were used to estimate the parameters:

1. Hysteresis loop method. This method calculates the viscous damping from the intersection of the loop with the force axis.
2. Sine curve fit method. This method fitted sine curves to the data and used the resulting equations to calculate the parameters. This method is essentially a more refined approach to the first method since all the measured data is used, while only two data points per cycle were used for the first method.
3. Hysteresis loop area method. This method calculates the loss factor from the area of the hysteresis loop.

The stiffness and loss factor are time dependent properties. Relaxation in stiffness occurs and this could have a major influence on the absorber's performance. It is assumed that the properties will decay exponentially until a stable value is reached. An exponential decay function was fitted to the data to extract the initial and stable values.

It is necessary to condition the data before use by:

1. De-trending the data by subtracting the average offset.
2. Filtering the data using a low pass digital filter with a cut off frequency set at 1.5 times the excitation frequency to reduce the influence of high frequency noise.
3. Calibrating the data with the appropriate factors.

4.2.1 Hysteresis loop equation method

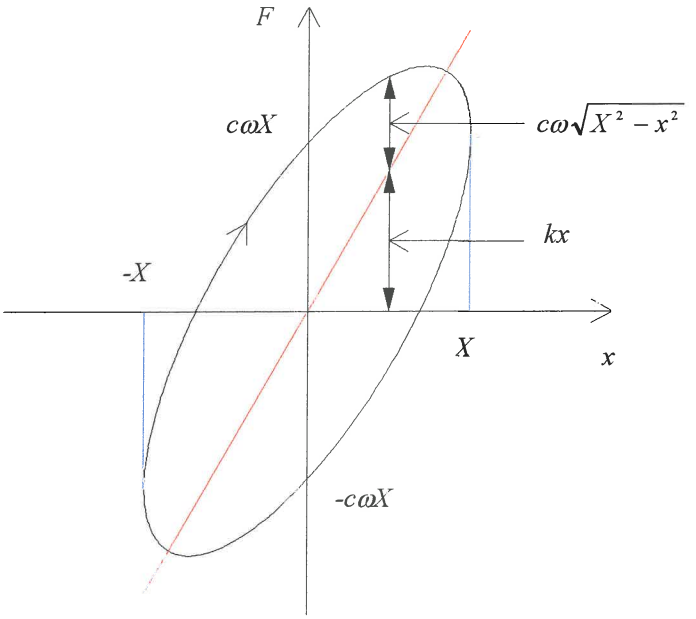

Figure 4.2 Hysteresis loop

The viscous hysteresis loop is described by Rao (1990):

$$f(t) = kx \pm c\omega\sqrt{X^2 - x^2} \tag{4.1}$$

in which x is:

$$x(t) = X \sin \omega t \tag{4.2}$$

From equation 4.1 it can be seen that the force at maximum displacement is given by:

$$f_{x=X} = kX \tag{4.3}$$

The force at zero displacement is given by:

$$f_{x=0} = \pm c\omega X \tag{4.4}$$

Equation 4.2 was implemented as shown below:

$$\sum_{i=1}^{n} |f_i|_{x=0} = c\omega \sum_{i=1}^{n} |X_i| \tag{4.5}$$

where n is the number of displacement peaks and troughs in the data set. X_i is the maximum and minimum displacement of the i-th peak or trough identified from the displacement time data. The extrema are identified from a change in the sign of the slope (figure 4.3).

The example in figure 4.3 shows the peaks identified at 15 Hz excitation. The number of peaks and troughs identified (n) varied between 29 and 30 for 15 Hz because there were not always 15 complete waves due to the excitation frequency that drifted slightly.

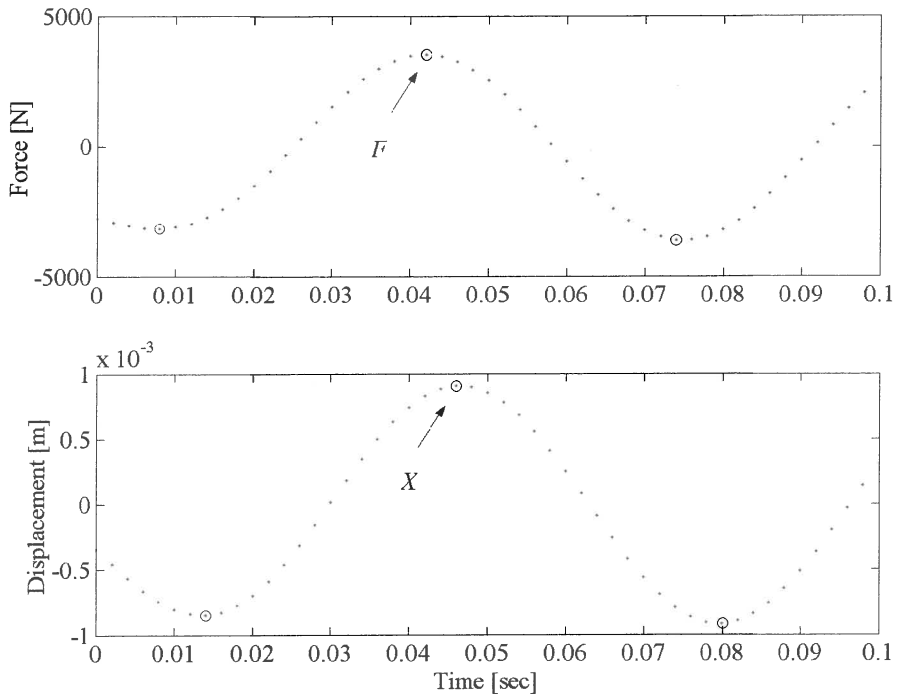

Figure 4.3 Peaks and troughs identified from the time data

f_i at $x = 0$ was determined by finding two data points between which the sign of the displacement changed. The exact time was then calculated through linear interpolation:

$$t_{x=0} = \frac{-x_k}{x_{k+1} - x_k}(t_{k+1} - t_k) + t_k \qquad \textbf{(4.6)}$$

The force at $x = 0$ could now be computed using this time point and the force time data:

$$f_{x=0} = \frac{t_{x=0} - t_k}{t_{k+1} - t_k}(f_{k+1} - f_k) + f_k \qquad \textbf{(4.7)}$$

The force and displacement data was captured simultaneously.

In equation 4.5 the excitation frequency was calculated by determining the frequency of maximum energy of a power spectral density calculation (PSD) of the displacement time data. The resolution of the PSD is 1 Hz. Figure 4.4 shows the PSD and illustrates the implementation of the low pass digital filter with a cut-off frequency of 1.5 times the excitation frequency.

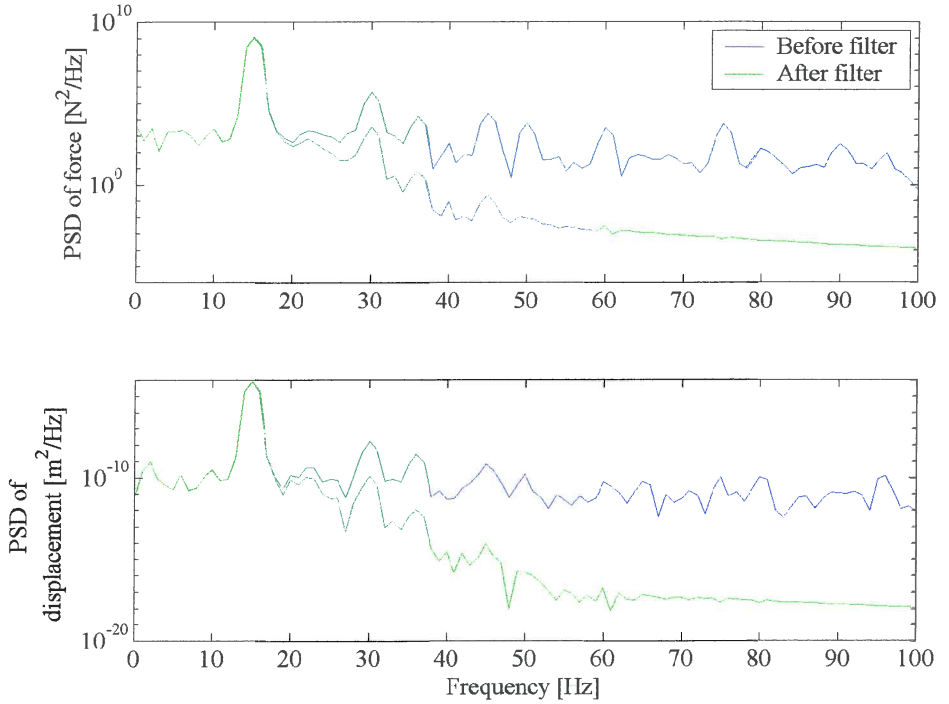

Figure 4.4 PSD of force and displacement data clearly showing the excitation frequency at 15 Hz as well as the effect of the low pass filter with a cut-off frequency at 22.5 Hz

c can be calculated using:

$$c = \frac{\sum_{i=1}^{n} |f_i|_{x=0}}{\omega \sum_{i=1}^{n} |X_i|} \tag{4.8}$$

The stiffness coefficient can be calculated by dividing the force at maximum displacement by the maximum displacement as follows:

$$k = \frac{\sum_{i=1}^{n} |f_i|_{x=X}}{\sum_{i=1}^{n} |X_i|} \tag{4.9}$$

The force at maximum displacement was found using the time at which the maximum displacement occurred as shown in figure 4.5. These values were averaged as shown in equation 4.9. The hysteretic damping can be calculated using:

$$h = c\omega \tag{4.10}$$

The loss factor is:

$$\eta = \frac{h}{k} \tag{4.11}$$

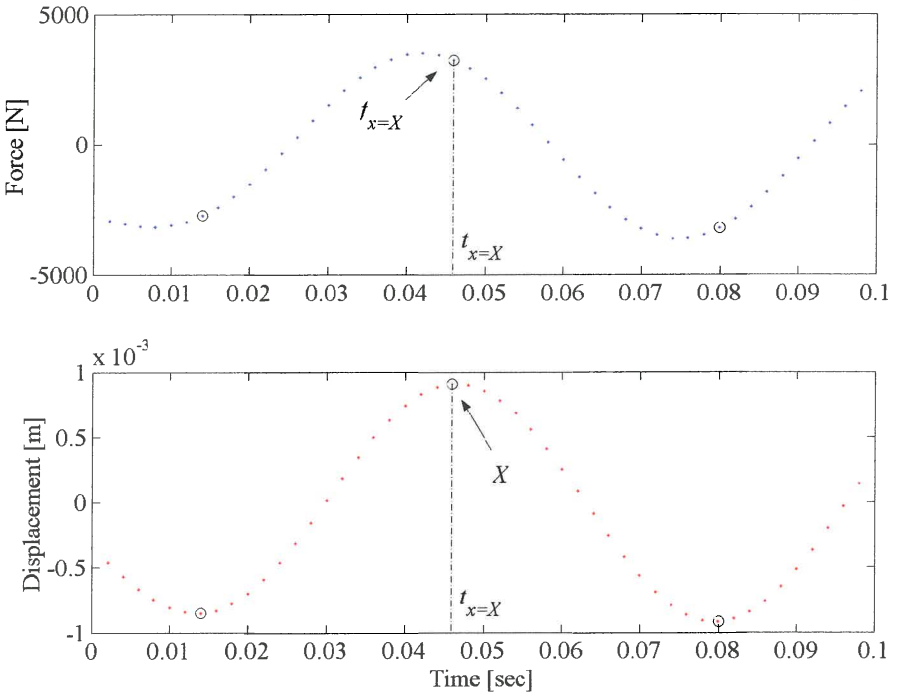

Figure 4.5 The force at maximum displacement ($x = X$)

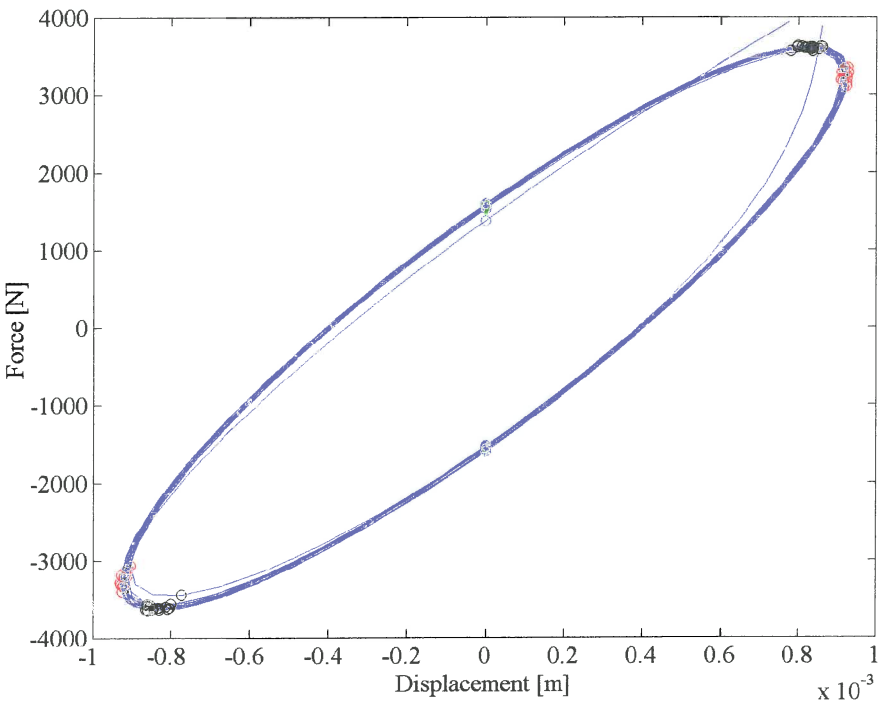

Figure 4.6 A typical hysteresis plot at 15 Hz excitation showing the force at minimum and maximum displacement (red), the minimum and maximum force (black) and the force at zero displacement (green) for each wave

4.2.2 Sine curve fit method

This method attempted to fit a sine curve through the data using an optimisation algorithm. The sine curve is described by the amplitude (A), the excitation frequency (ω) and the phase angle (ϕ):

$$y = A\sin(\omega t + \phi) \tag{4.12}$$

The objective function is:

$$f(\bar{x}) = \sum_{i=1}^{m}(x_1 \sin(x_2 t_i + x_3) - y_i)^2 \tag{4.13}$$

where $m = f_s \Delta t$ is the total number of data points (y_i) measured. This was done twice for each set of data, once for the force data and once for the displacement data. The MATLAB `fminsearch.m` algorithm was used. This algorithm uses an unconstrained Nelder-Mead type simplex search method. The initial values for the amplitude and frequency were taken from the results of previous method (§4.2.1) and the phase angle was chosen as zero. It was found that convergence was not always achieved and in such cases it was remedied by restarting the optimisation using a random phase angle in the interval [-2π,2π].

The convergence criteria where:

- a positive amplitude (A),
- the value of the objective function must be less than an acceptable value (which was found through trial and error), and
- the difference between the current and a previous value for the objective function should be less than 1×10^{-5}.

The fitted parameters for the displacement are shown in equation 4.14.

$$x(t) = A_x \sin(\omega_x t + \phi_x) \tag{4.14}$$

The fitted parameters for the force are shown in equation 4.15.

$$f(t) = A_f \sin(\omega_f t + \phi_f) \tag{4.15}$$

The time at which the displacement is zero can now be calculated from the fitted parameters:

$$t_{x=0} = -\frac{\phi_x}{\omega_x} \tag{4.16}$$

The force at zero displacement is therefore:

$$f_{x=0} = A_f \sin\left(-\omega_f \frac{\phi_x}{\omega_x} + \phi_f\right) \tag{4.17}$$

The force at maximum displacement can be found by adding a quarter of the period to the time at zero displacement:

$$f_{x=X} = A_f \sin\left[\omega_f\left(-\frac{\phi_x}{\omega_x}+\frac{\pi}{2\omega_x}\right)+\phi_f\right] \tag{4.18}$$

The damping can now be calculated with ω taken as the average of two fitted values:

$$c = \frac{f_{x=0}}{\omega A_x} \tag{4.19}$$

The stiffness is:

$$k = \frac{f_{x=X}}{A_x} \tag{4.20}$$

The values of h and η can be found from equation 4.10 and 4.11.

It is also possible to find the loss factor (η) from the difference in the phase angle between the two signals:

$$\eta = \tan(\phi_f - \phi_x) \tag{4.21}$$

4.2.3 Hysteresis loop area method

The hysteresis loop area method estimates the energy loss per cycle. The area of the loop is equal to the amount of energy dissipated. The area is calculated using the trapezium method. The area of the loop is:

$$Area = \frac{1}{n}\sum_{i=1}^{m}\frac{f_{i+1}+f_i}{x_{i+1}-x_i} \tag{4.22}$$

n is the number of complete loops found. m is the total number of sampling points for n loops. The energy loss is related to the hysteretic damping by:

$$\Delta W = \pi h X^2 \tag{4.23}$$

The hysteretic damping is:

$$h = \frac{Area}{\pi X^2} \tag{4.24}$$

The loss factor (η) can be found using equation 4.11

4.2.4 Relaxation

The properties of the polyurethane changes with time. The initial values are denoted k_0 and η_0 and the stable values k_∞ and η_∞. It is assumed that it will decay exponentially from the initial value until a stable value is reached:

$$k(t) = k_0 e^{-dt} + k_\infty \tag{4.25}$$

A non-linear least-squares data fitting procedure using the Gauss-Newton method (`nlinfit.m`) in the MATLAB statistics toolbox was used to fit the model described by equation 4.26 to the observed data. A good fit was not always obtained.

$$y = \beta_1 e^{-\beta_2 t} + \beta_3 \tag{4.26}$$

This method also returned the residuals and the Jacobian, which can be used to find the confidence interval with the function `nlpredci.m`. Figure 4.7 shows a typical good fit of stiffness.

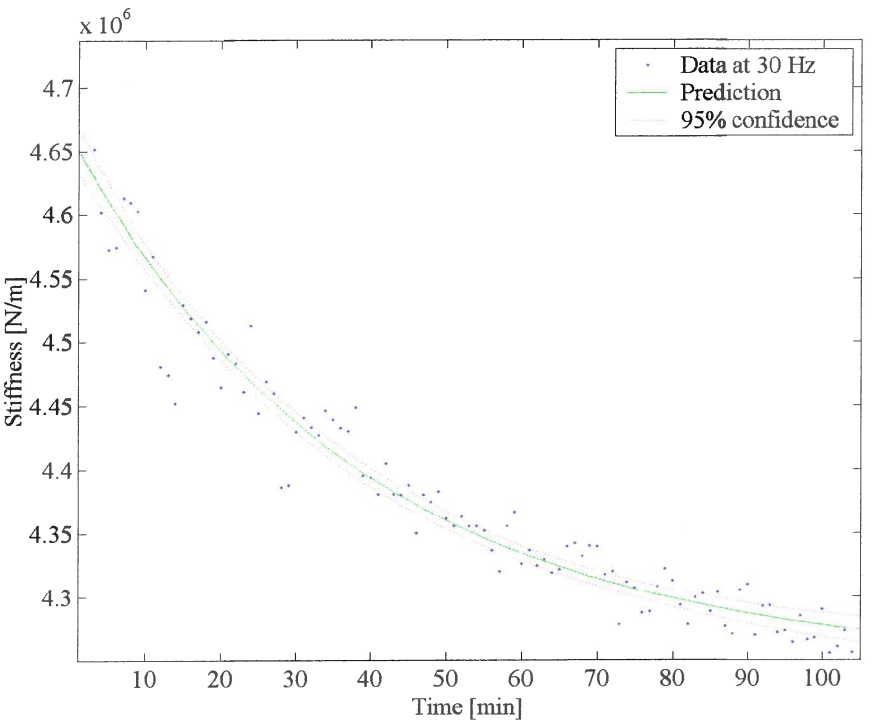

Figure 4.7 The stiffness (k) as a function of time

4.3 Sine sweep excitation

The sine sweep is a sinusoidal command signal, the frequency of which is varied slowly but continuously through the range of interest (Ewins, 1995). It is necessary to check that the progress through the frequency range is slow enough that steady-state conditions are attained before measurements are made. If excessive sweep rates are used the measured FRF is distorted. One way of checking the suitability of a sweep rate is to make two measurements, one sweeping up and another sweeping down. If the same curve is obtained then there is a possibility, though not a certainty, that the sweep rate is not excessive.

It is possible to prescribe an optimum sweep rate for a given structure. In theory any sweep rate is too fast to guarantee that the full steady-state response level will be attained, but in practice it is possible to attain a condition very close to this desired state. ISO 7626 suggest the following maximum sweep rates.

$$S_{\max} < 54 f_r^2 \eta_r^2 \quad \text{or} \quad S_{\max} < 216 f_r^2 \zeta_r^2 \tag{4.27}$$

For the experimental test set-up a worst case would be:

- $f_r = 20$ Hz
- $\eta_r = 0.2$

The maximum sweep rate would therefore be 864 Hz/min. For the desired 70 Hz sine sweep should therefore not be completed in less than 4.86 seconds.

4.3.1 Transfer function estimate of the stiffness and loss factor

The amplitude of the displacement and the force transmitted to the top load cell were used to calculate the stiffness and the loss factor:

$$\frac{F_o}{X} = k(1 + i\eta) \tag{4.28}$$

The transfer function between the force and the displacement is an estimate of the amplitude ratio:

$$\frac{F_o}{X} = \frac{S_{f_o f_o}(\omega)}{S_{f_o x}(i\omega)} \tag{4.29}$$

The transfer function is estimated in MATLAB with the `tfe.m` function using Welch's averaged periodogram method.

The stiffness is:

$$k_s(\omega) = \mathrm{Re}\left(\frac{F_o}{X}\right) \tag{4.30}$$

The loss factor is calculated as follows:

$$\eta_s(\omega) = \frac{\mathrm{Im}\left(\frac{F_o}{X}\right)}{k_s(\omega)} \tag{4.31}$$

The displacement signal was modified to compensate for the control system's inability to provide the required amplitude at higher frequencies and to reduce the response at resonance. This was done through trial and error. The best response was obtained using the amplitude shown in figure 4.8.

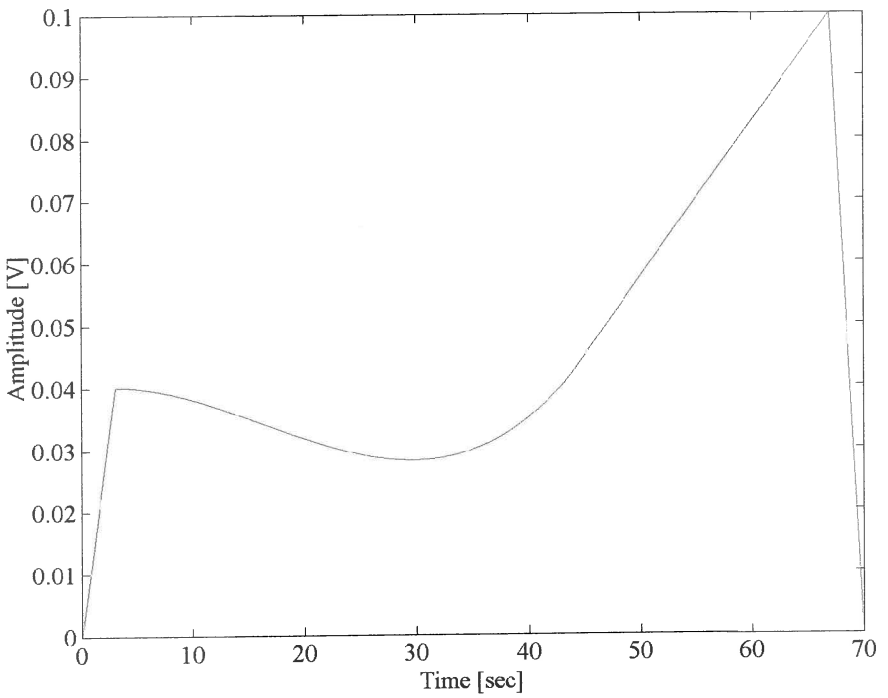

Figure 4.8 Modified time signal amplitude

A typical moving average envelope of the displacement for a 70-second sine sweep is shown in figure 4.9.

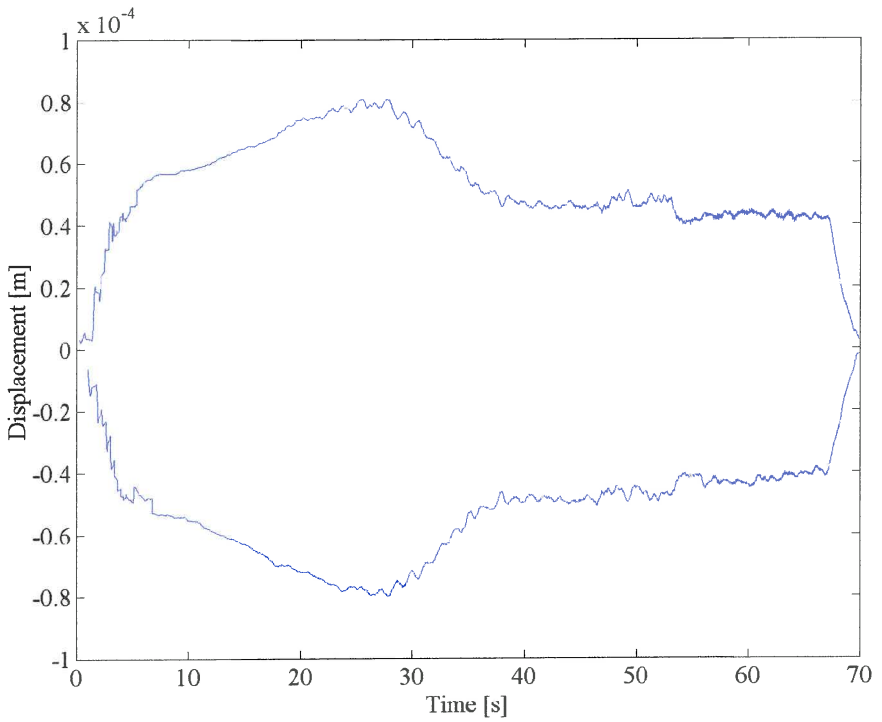

Figure 4.9 Actual measured displacement envelope (20 point moving average)

4.3.2 Transmissibility

The transmissibility was calculated using the transfer function estimate as was done in equation 4.29.

$$\frac{F_o}{F_i} = \frac{S_{f_o f_o}(\omega)}{S_{f_o f_i}(i\omega)} \tag{4.32}$$

This was done for an absorber filled with liquid as well as for an unfilled absorber which, highlighted the change in system's response. For the filled absorber the system characteristics can be extracted from the measured transmissibility data by finding the parameters that best represents the transmissibility curve with an optimisation procedure. Fitting all the parameters at once proved impossible. However, the system's mass (m), geometry and absorber fluid density was known and only the stiffness, loss factor and viscous damping needed to be calculated. The loss factor was estimated as 0.1 from previous tests to further simplify the analysis. The stiffness is a linear function of frequency for the frequency range of interest:

$$k(\omega) = k_1\omega + k_2 \tag{4.33}$$

In chapter 2 the viscous damping was found to be a linear function of frequency which must be zero when the port velocity is zero:

$$c(\omega) = c_1 \omega \tag{4.34}$$

The model of the transmissibility used for the curve fit is therefore:

$$T_r = \frac{(x_1\omega + x_2)(1+i\eta) + i\omega^2 x_3 + \omega^2 m_B \left(1 - \frac{A_b}{A_a}\right)\frac{A_b}{A_a}}{(x_1\omega + x_2)(1+i\eta) + i\omega^2 x_3 - \omega^2 \left[m + m_B\left(1 - \frac{A_b}{A_a}\right)^2\right]} \tag{4.35}$$

MATLAB does not specifically allow for complex optimisation and therefore the absolute value and phase angle of the transmissibility was used to define the objective function as a multiple objective optimisation problem. The square of the difference in the absolute value and phase angle at each measurement point is compared and the sum of the differences is minimised.

$$f(\bar{x}) = w_1 \sum_{i=1}^{n} \left(|(T_r)_i| - |(T_r^m)_i| \right)^2 + w_2 \sum_{i=1}^{n} \left(\angle(T_r)_i - \angle(T_r^m)_i \right)^2$$

subject to

$$g_i(\bar{x}) = -x_i \le 0 \qquad i = 1,2,3 \tag{4.36}$$

where T_r^m is the measured data, n the number of sampling points used and w_1 and w_2 weight assigned to the objectives. The values of all the variables had to be greater than zero since they are physical properties. It is not necessary to include all the sampling points for the optimisation, especially data at low frequencies where the measurements can be inaccurate. It is recommended that most of the points measured close to the maximum transmissibility and isolation are included.

The weights were chosen through trial and error and it was found that the contribution of both these functions were of the same order. Visual inspection of the fit is recommended to ensure that both the absolute value and phase angle are fitted successfully.

The constrained non-linear optimisation algorithm `fmincon.m` was used to minimise the objective function.

4. Results

4.4.1 Stiffness

The relaxation data for the hysteresis loop equation and the sine curve fit are compared in figure 4.10. Both methods showed some scatter, but the trend is clear.

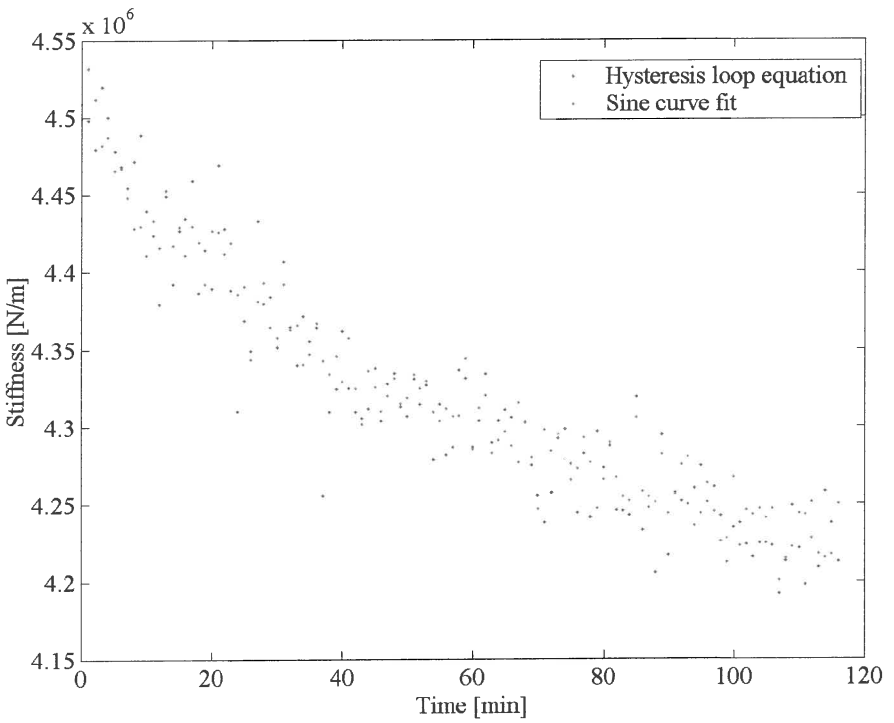

Figure 4.10 Stiffness compared (35 Hz)

In figure 4.7 an example of a relaxation curve fit was shown. Not all these curve fits were successful due to excessive scatter in the data (refer to appendix G). An average of the successful fits were used to determine the initial and stable values for the stiffness at the measured frequencies. The amount of relaxation that occurred was between 1 and 9%. This drift in stiffness will result in a change in the isolation frequency. In practice, some form of compensation will be necessary. These values are shown in figure 4.11 together with the stiffness determined from the sine sweep.

Table 4.1 Comparison of straight-line curve fits in figure 4.11 (55 Shore A spring)

Stiffness		Slope [$\times 10^3$]	Ordinate [$\times 10^6$]
Initial stiffness	k_0	8.88	2.74
Stable stiffness	k_∞	7.97	2.69
Sine sweep	k_s	11.36	2.48

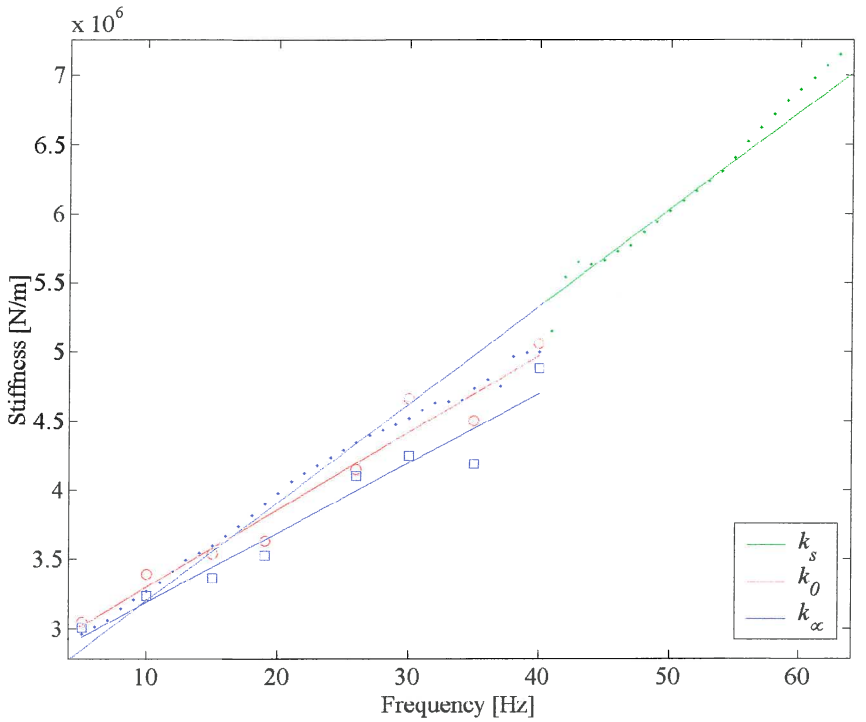

Figure 4.11 The stiffness of the 55 Shore A spring calculated with the sine sweep method (green) and the initial (red) and stable (blue) stiffness calculated with the constant frequency excitation method

The results of the two methods differ slightly. The sine sweep and initial stiffness data below 40 Hz showed excellent correlation. The sine sweep method at the 1 Hz per second sweep rate is therefore deemed to be adequate for the calculation of the initial spring stiffness.

The relaxation test was very time consuming and was not repeated for the 35 Shore A spring. Instead 10 seconds of time data was sampled at 1000 Hz from 10 to 55 Hz and was used to calculate the stiffness using the constant frequency excitation methods. The transient run-up and run-down sections of the data were ignored and only the steady state portion was used for the calculation. The curve fits are compared in figure 4.12. The spring was approximately 40% softer than the 55 Shore A spring at 0 Hz while the slope was ±20% less. 35 Shore A is the softest polyurethane that was available and this represents the lowest stiffness value achievable using this material and geometry.

Table 4.2 Comparison of straight-line curve fits in figure 4.12 (35 Shore A spring)

Stiffness		Slope [$\times 10^3$]	Ordinate [$\times 10^6$]
Initial stiffness	k_0	7.29	1.62
Sine sweep	k_s	6.74	1.72

The static stiffness of the 35 Shore A spring was 1.28×10^6 N/m

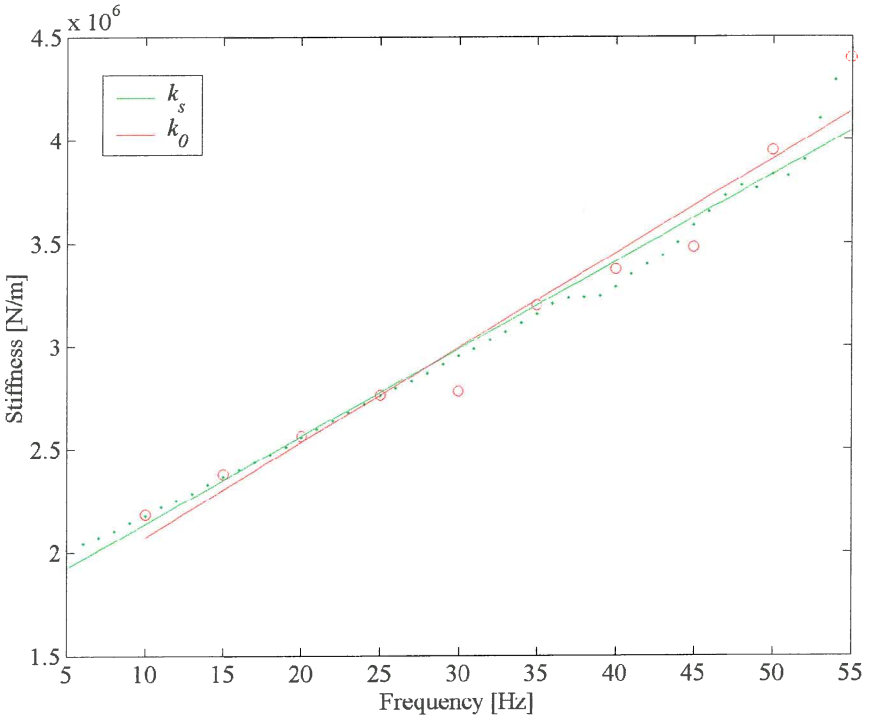

Figure 4.12 The stiffness of the 35 Shore A spring calculated with the sine sweep method (green) and the initial stiffness calculated with the constant frequency excitation method (red)

4.4.2 Loss factor

The results for the loss factor were less successful than for stiffness. Although the methods showed good agreement, admittedly with some scatter, it was generally higher than expected (figure 4.13). It is concluded that the phase angle measurement did not accurately represent the material but was influenced by the absorber assembly. A 40 mm cube of the same material was tested (figure 4.14) and the loss factor was closer to the 0.1 that was expected from published values by DuPont for Hylene®PPDI (a similar polyurethane) and the 60 shore A results measured at the University of Pretoria. The tests did show that the loss factor was not a function of frequency. The loss factor did also not show any relaxation as the stiffness did as can be seen in figure 4.15 which shows a typical curve fit.

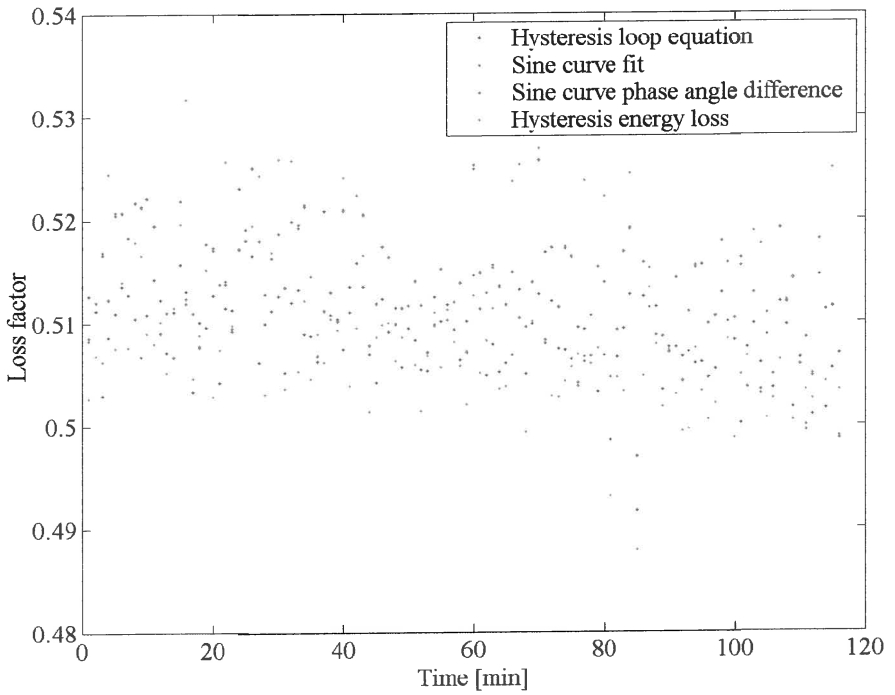

Figure 4.13 Comparison of the loss factor using four methods (35 Hz)

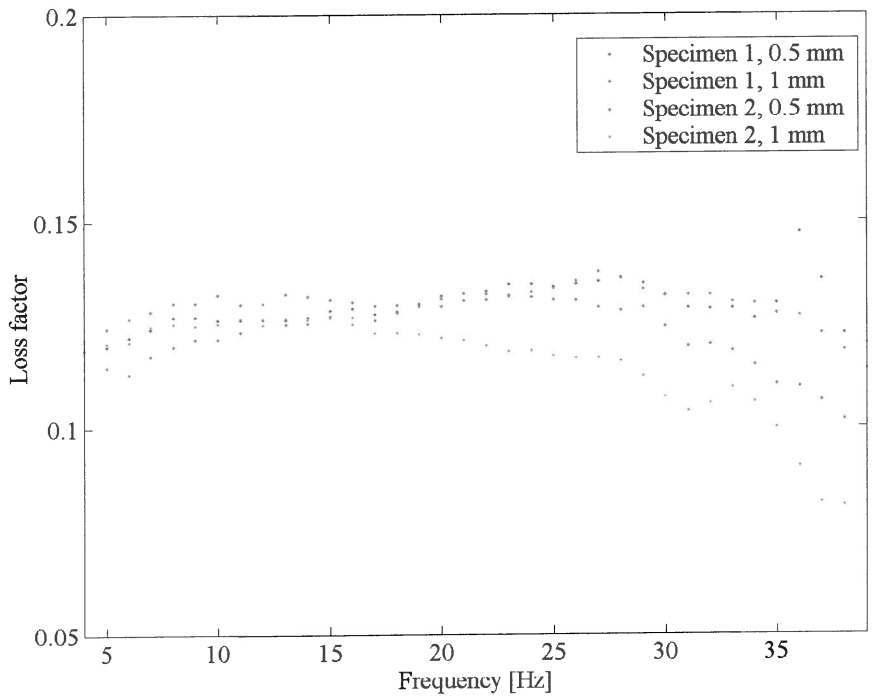

Figure 4.14 The loss factor for 2 cubic specimens at 0.5 mm and 1 mm displacements

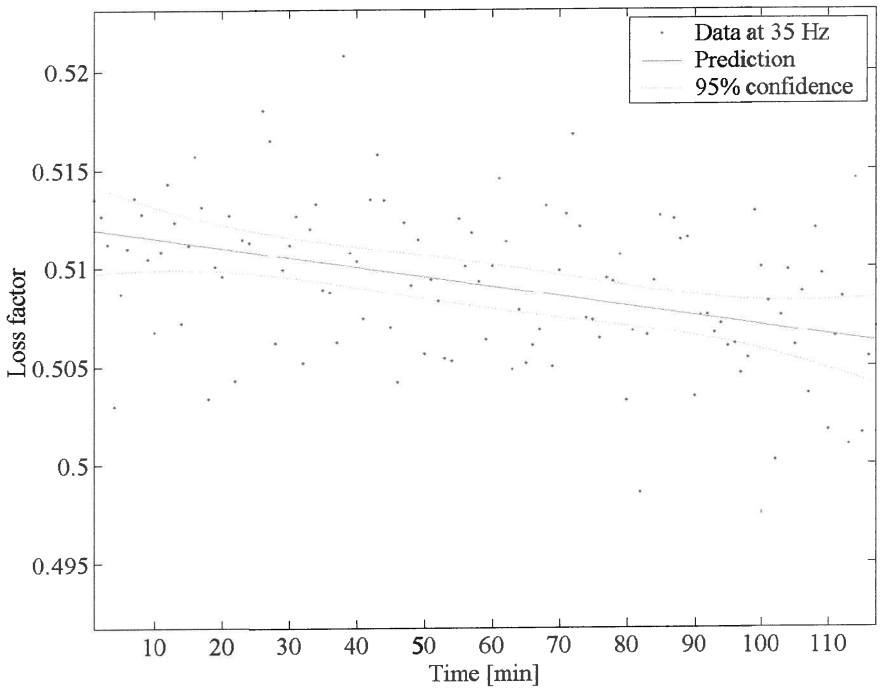

Figure 4.15 An unsuccessful curve fit of the loss factor for the absorber

4.4.3 Transmissibility

The transmissibility was measured with and without the absorber fluid to highlight the dramatic reduction in the force transmitted (figures 4.16 and 4.17). As expected the 35 Shore A spring had better isolation and a lower isolation frequency. The characteristics are shown in table 4.3

Table 4.3 Absorber characteristics

Spring hardness [Shore A]		Frequency [Hz]	$\lvert T_r \rvert$
55	Maximum response	39	2.07
	Isolation	49	0.45
35	Maximum response	33	1.77
	Isolation	42	0.16

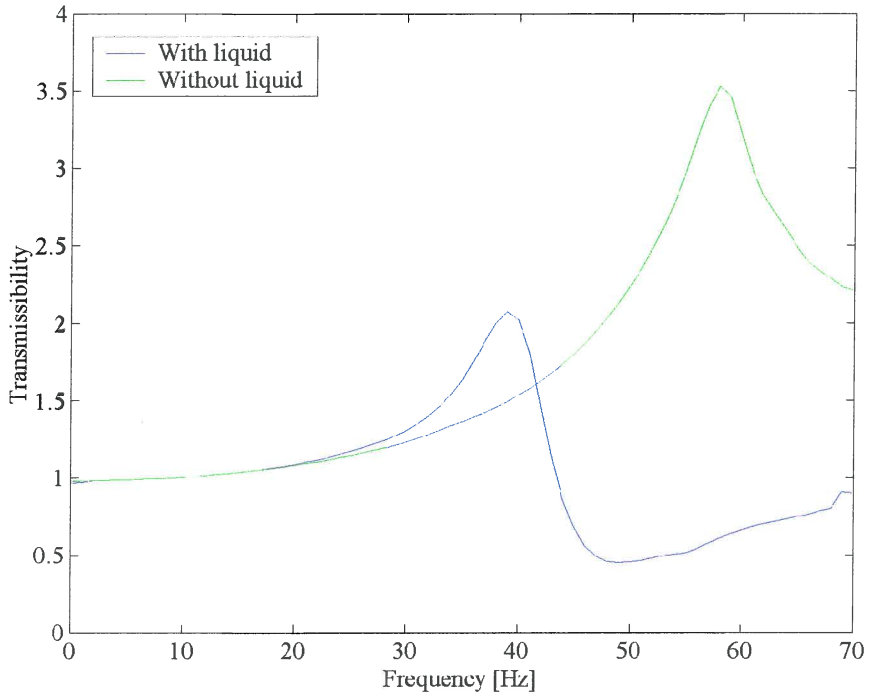

Figure 4.16 Comparison of the transmissibility for the 55 Shore A spring before and after the addition of the absorber liquid

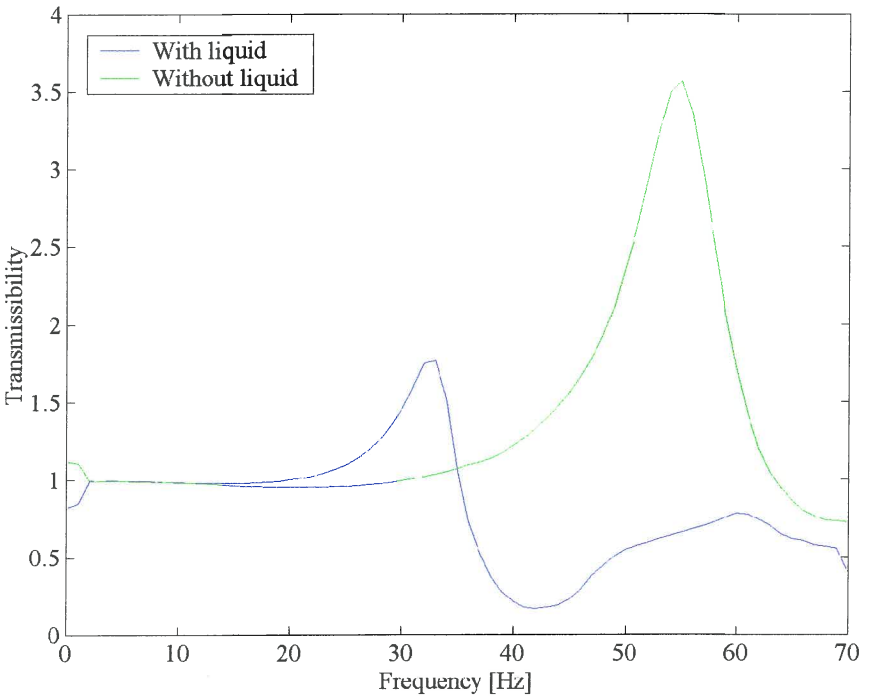

Figure 4.17 Comparison of the transmissibility for the 35 Shore A spring before and after the addition of the absorber liquid

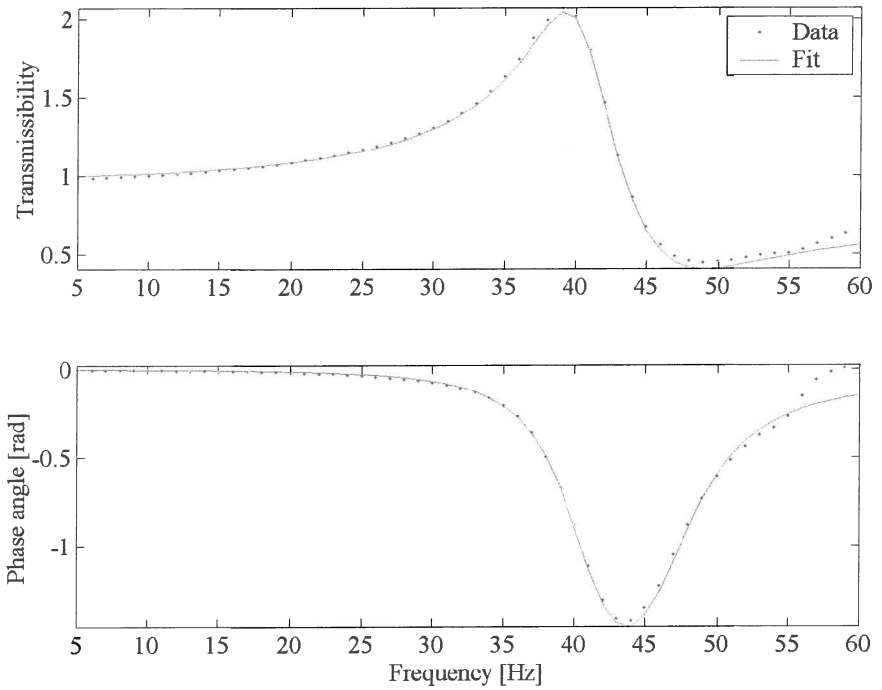

Figure 4.18 The 55 Shore A spring curve fit with $\eta = 0.1$ $m = 15$

Figure 4.18 shows the fit obtained using equation 4.36. The values obtained for the stiffness and damping were:

$$k_t(\omega) = 0.43 \times 10^4 \omega + 2.88 \times 10^6 \quad \textbf{(4.37)}$$

$$c_t(\omega) = 2.23\omega \quad \textbf{(4.38)}$$

The objective function could not be fitted successfully the 35 shore A spring's transmissibility data.

4.5 Conclusion

The methods used to characterise the absorber are in good agreement and it can be concluded that they are sound. The quality of the measured data was in some cases insufficient to obtain good fits of theoretical predictions. Halwes (1980) concluded that the properties of the elastomer could not economically be controlled to within ±10% of the target value. This study reiterated that the major obstacle for mass production of these absorbers would be the type of elastomer used. In practice changes to the port diameter after the manufacture of the spring will be necessary. Halwes did this by specifying the port diameter at the maximum stiffness expected. The spring stiffness was measured after manufacture and the port was reamed to compensate if the spring rate was less.

The transmissibility data clearly shows that the absorber can reduce the force transmitted by a single degree-of-freedom system significantly. The 35 Shore A spring reduced the isolation frequency by 7 Hz. The measurement techniques must be improved if accurate parameter extraction is desired.

CHAPTER 5

Design study

5.1 Introduction

In this chapter a vibration absorber will be designed for a screen application. The design methodology described in chapter 3 will be used, but in this case the isolation frequency will be 12.5 Hz. The chosen screen was designed for a sand washing plant. First the single degree-of-freedom screen model will be analysed. Then an absorber will be added. The effect will be discussed. Next a two degree-of-freedom screen model will be designed according to the SDRC guidelines given in chapter 1 (Riddle *et al.*, 1984). An absorber will then be added between the sub-frame and the ground to illustrate the improvement possible. To simplify the comparison, hysteretic damping will be assumed for both the screen and the absorber. The screen is fitted on steel coil springs with a loss factor of 0.01. It is further assumed that the combined viscous and material damping of the absorber can be represented by a loss factor of 0.1.

Finally the study will be concluded with recommendations for the design of absorbers for screens.

5.2 Single degree-of-freedom screens

5.2.1 Screen

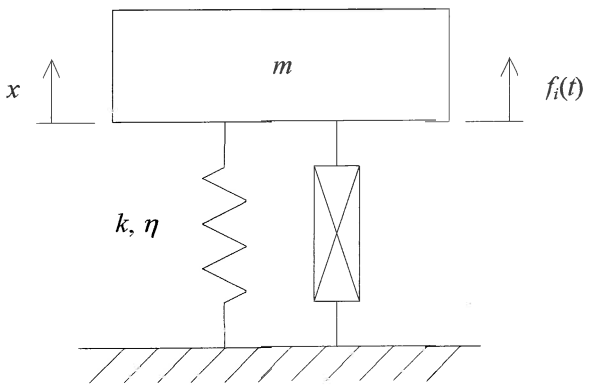

Figure 5.1 A single degree-of-freedom screen

According to the manufacturer two rotating eccentric mass excitation motors transfer 27 000 kg of force to the screen. The motors rotate at 750 rpm. The spring rate is given as 30.4 kg/mm and there are 4 springs on each corner. The screen has a 2-second run-up time, which is too short for any problematic transient response amplification. Run-down can take as long as 2 minutes and damping can therefore become important to reduce the response at resonance.

Table 5.1 Physical properties of the screen

Mass [kg]	m	13×10^3
Force amplitude[1] [N]	F_i	264.87×10^3
Stiffness[2] [N/m]	k	4.77×10^6
Spring loss factor	η	0.01
Operating speed [Hz]	f	12.5

[1] 27000×9.81, [2] $4\times4\times30.4\times10^3\times9.81$

Table 5.2 Operating characteristics the screen

Natural frequency [Hz]	f_n	3.05
Frequency ratio	$\frac{\omega}{\omega_n}$	4.1
Stroke amplitude [mm]	X	3.5
Acceleration [m/s^2]	$\omega^2 X$	2.21g
Static deflection [mm]	x_s	26.7
Dynamic force transmitted [N]	F_o	16758.55
Transmissibility [%]	$\lvert T_r \rvert$	6.327

Figures 5.2 and 5.3 show the response and force transmissibility of this design. The low damping of the spring can cause high amplitudes at the natural frequency during run-down.

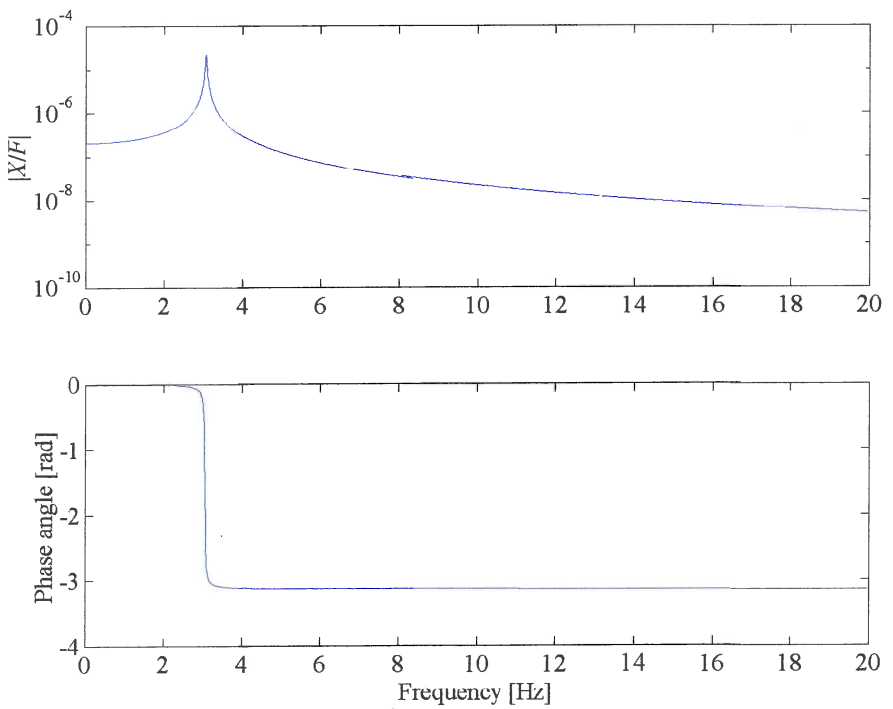

Figure 5.2 Response of the screen

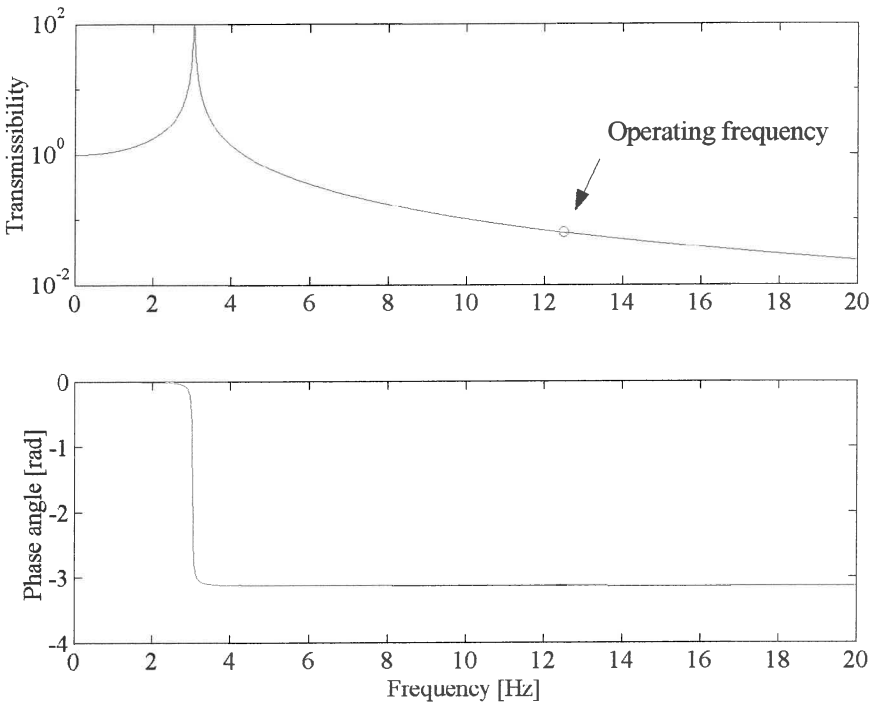

Figure 5.3 Transmissibility of the screen

The design of the screen was done in accordance with current practice and therefore the operating frequency is 4 times larger than resonance. Although the transmissibility is only 6%, a total of 16.8 kN is still transmitted to the support structure.

5.2.2 Screen with an absorber

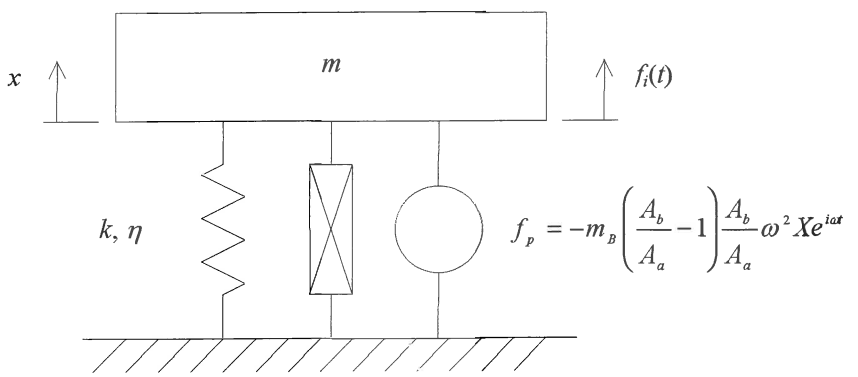

Figure 5.4 Screen fitted with a LIVE absorber

The force f_p in figure 5.4 is the force generated by the absorber (equation 2.59).

In chapter 3 it was shown that the best isolation would be achieved when the stiffness of the spring is as low as possible. For the screen application low stiffness would result in high static deflection. For a steel spring the static deflection will only become problematic at 125 mm (chapter 1). The LIVE absorber cannot accommodate high static deflection easily. The first problem is the available space, but more importantly the polyurethane's ultimate tensile strength must not be exceeded. Both these problems can be overcome if the static deflection is reasonably low. The experimental absorber was built to deflect only 10 mm, but with a softer material and a different geometry it will be possible to attain larger deflections. It is thought that a 20 mm deflection can still be accommodated in a design. The results are therefore listed for the best possible 20 mm deflection as well as for 26.7 mm in order to compare it to the previous result for the screen. The absorber was designed in accordance with the guidelines in chapter 3. The mass, force and forcing frequency is the same as before.

Table 5.3 Physical properties of the system

		$x_s = 20$	$x_s = 26.7$
Mass [kg]	m	13×10^3	13×10^3
Force amplitude [N]	F_i	264.87×10^3	264.87×10^3
Stiffness [N/m]	k	6.38×10^6	4.78×10^6
Spring loss factor	η	0.1	0.1
Operating speed [Hz]	f	12.5	12.5
Area ratio	A_r	36	36
Reservoir diameter [mm]	d_b	180	180
Absorber liquid density [kg/m^3]	ρ	1000	1000

Table 5.4 Design results and operating characteristics of the system

		$x_s = 20$	$x_s = 26.7$
Port length [mm]	l	290	217
Port diameter [mm]	d_a	30	30
Natural frequency [Hz]	f_n	3.52	3.05
Frequency ratio	$\frac{\omega}{\omega_n}$	3.55	4.1
Stroke amplitude [mm]	X	3.64	3.64
Acceleration [m/s^2]	$\omega^2 X$	2.29g	2.29g
Dynamic force transmitted [N]	F_o	2322	1738
Transmissibility [%]	$\lvert T_r \rvert$	0.797	0.597

At a static deflection of 20 mm the force transmitted to the support structure is 7.2 times less than a screen fitted with conventional isolators. Figures 5.5 and 5.6 show the response and transmissibility for the design.

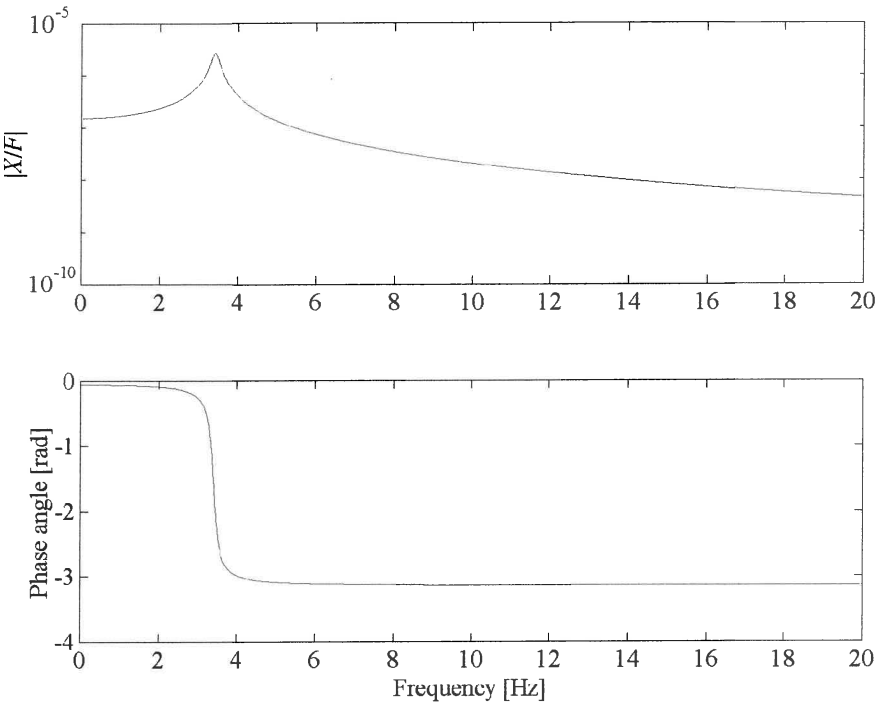

Figure 5.5 Response of the screen with an absorber fitted ($x_s = 20$ mm)

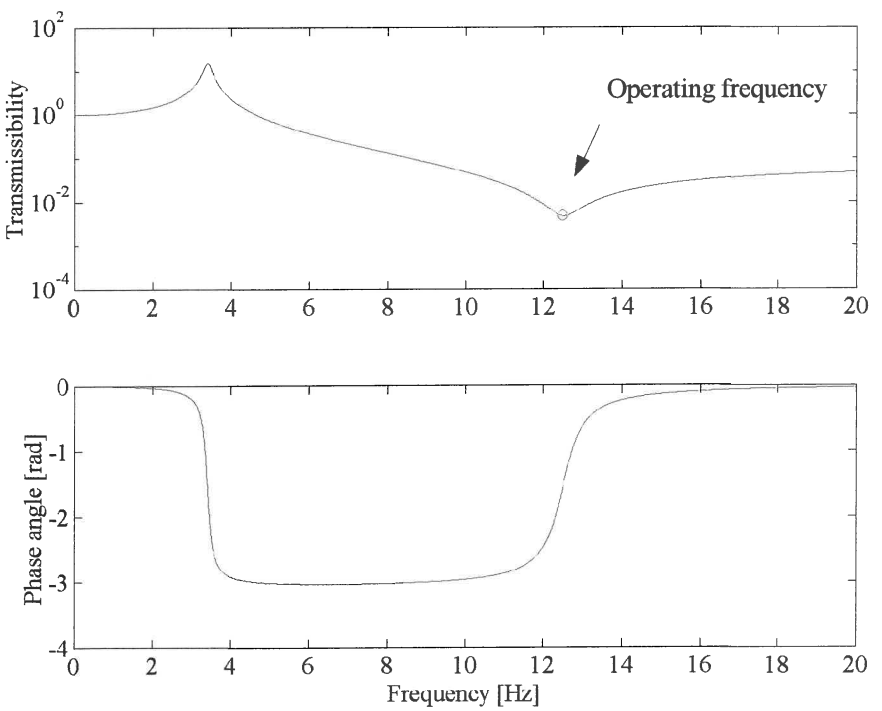

Figure 5.6 Transmissibility of a screen with an absorber fitted ($x_s = 20$ mm)

5.3 Two degree-of-freedom screens

5.3.1 Screen with a sub-frame

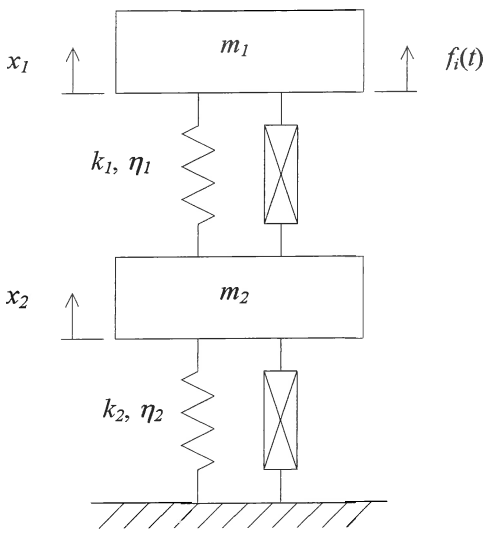

Figure 5.7 Screen with a sub-frame

Table 5.5 Physical properties of the screen with a sub-frame

		$x_2 = 20$ mm	$x_2 = 37.5$ mm
Screen mass [kg]	m_1	13×10^3	13×10^3
Sub-frame mass [kg]	m_2	16.9×10^3	16.9×10^3
Mass ratio	$\frac{m_2}{m_1}$	1.3	1.3
Screen stiffness [N/m]	k_1	4.77×10^6	4.77×10^6
Sub-frame stiffness [N/m]	k_2	14.67×10^6	7.82×10^6
Loss factor of the screen spring	n_1	0.01	0.01
Loss factor of the absorber spring	n_2	0.1	0.1
Static deflection of the screen [mm]	x_1	46.7	64.22
Stiffness ratio	$\frac{k_2}{k_1}$	3.07	1.64

The screen mass, stiffness, excitation force and frequency is the same as before. The sub-frame mass is 1.3 times the screen mass (chapter 1). The sub-frame stiffness was calculated using the permissible static deflection of a rubber spring, which was given as 15% of its free length (37.5 mm for a 250 mm spring) by Riddle *et al.* (1984).

Table 5.6 Operating characteristics of the screen with a sub-frame

		$x_2 = 20$ mm	$x_2 = 37.5$ mm
Natural frequencies [Hz]	f_1	2.53	2.15
	f_2	5.66	4.85
Frequency ratios	$\frac{\omega}{\omega_1}$	2.21	5.8
	$\frac{\omega}{\omega_2}$	4.94	2.57
Static deflection of the screen [mm]	x_1	46.7	64.2
Dynamic force transmitted [N]	F_o	2922	1442
Stroke amplitude [mm]	X_1	3.52	3.52
	X_2	0.198	0.183
Acceleration [m/s^2]	$\omega^2 X_1$	2.216g	2.215g
Transmissibility [%]	$\lvert T_r \rvert$	1.1	0.544

It will still be possible to achieve low transmissibility without using the upper bound of 130% of the screen mass for the sub-frame mass. Figure 5.8 shows that the gain in isolation will be less at high mass ratios. A 50% mass ratio will therefore already provide good isolation while not adding too much weight to the assembly. Figures 5.9 to 5.11 show the response and transmissibility for a system with a sub-frame deflection of 37.5 mm.

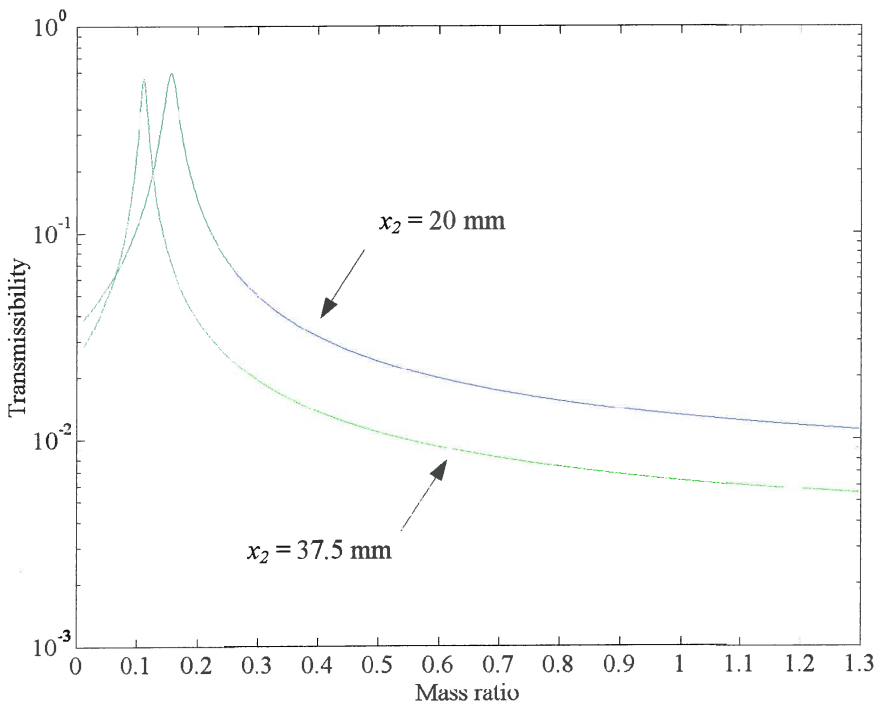

Figure 5.8 Transmissibility at 12.5 Hz as a function of mass ratio

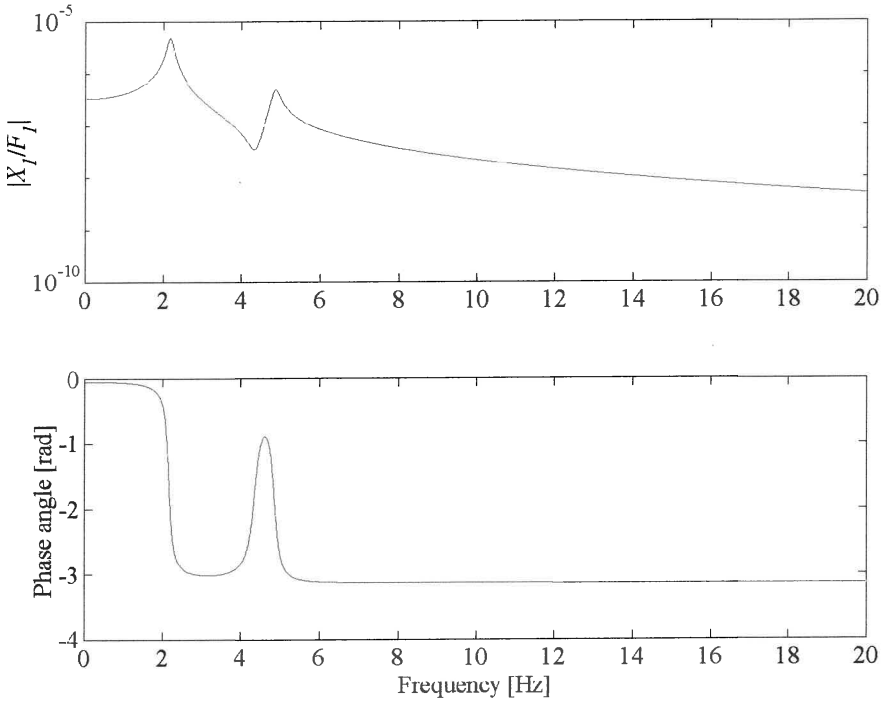

Figure 5.9 Response of the screen to the excitation force (x_2 = 37.5 mm)

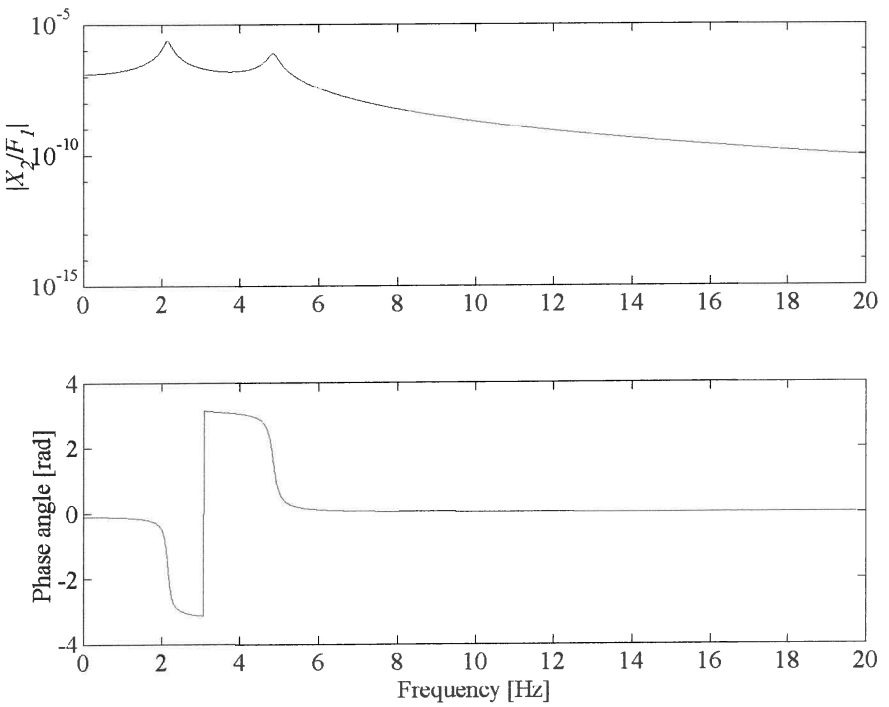

Figure 5.10 Response of the sub-frame to the excitation force (x_2 = 37.5 mm)

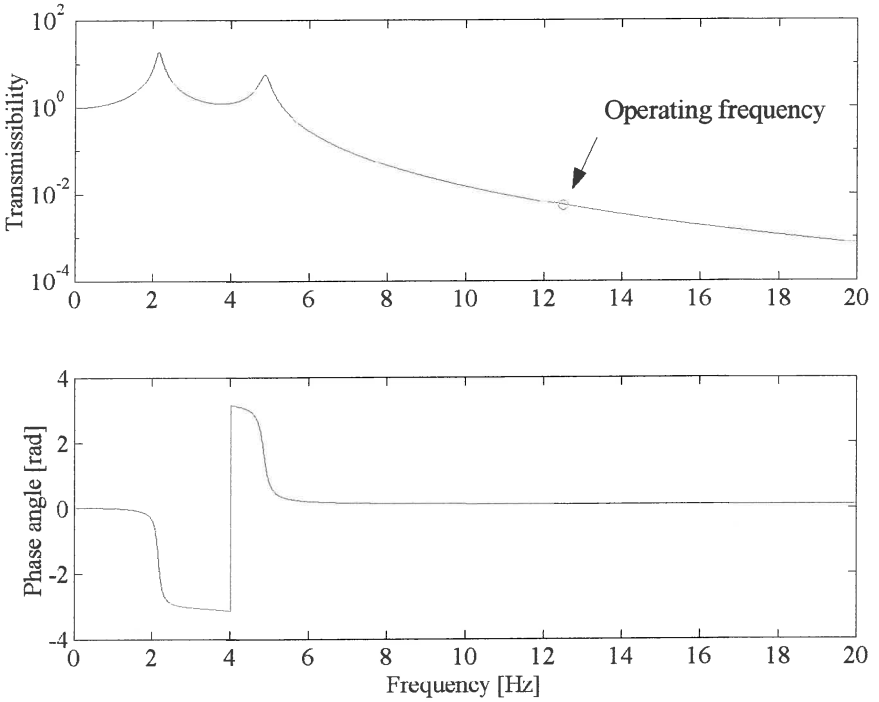

Figure 5.11 Transmissibility of a screen with a sub-frame (x_2 = 37.5 mm)

5.3.2 Screen with a sub-frame and an absorber

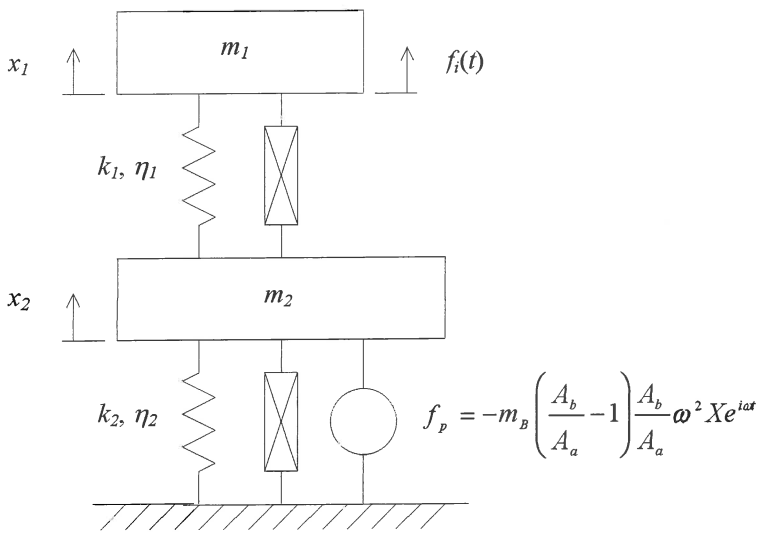

Figure 5.12 Screen with a sub-frame and a LIVE absorber

The force f_p in figure 5.12 is the force generated by the absorber.

Table 5.7 Physical properties of the system

		$x_2 = 20$ mm	$x_2 = 37.5$ mm
Screen mass [kg]	m_1	13×10^3	13×10^3
Secondary mass [kg]	m_2	1950	1950
Mass ratio	$\frac{m_2}{m_1}$	0.15	0.15
Screen stiffness [N/m]	k_1	4.77×10^6	4.77×10^6
Absorber stiffness [N/m]	k_2	7.33×10^6	3.91×10^6
Stiffness ratio	$\frac{k_2}{k_1}$	1.54	0.82
Loss factor of the screen spring	n_1	0.01	0.01
Loss factor of the absorber spring	n_2	0.1	0.1
Static deflection of the screen [mm]	x_1	46.7	64.22
Area ratio	A_r	36	36
Reservoir diameter [mm]	d_b	180	180
Absorber liquid density [kg/m^3]	ρ	1000	1000

Table 5.8 Design results and operating characteristics the system

		$x_2 = 20$ mm	$x_2 = 37.5$ mm
Port length	l	337	179
Port diameter	d_a	30	30
Natural frequencies [Hz]	f_1	2.33	1.99
	f_2	10.1	9.54
Frequency ratios	$\frac{\omega}{\omega_1}$	5.36	6.29
	$\frac{\omega}{\omega_2}$	1.23	1.31
Dynamic force transmitted [N]	F_o	1808	955
Stroke amplitude [mm]	X_1	3.67	3.67
	X_2	2.47	2.44
Acceleration [m/s^2]	$\omega^2 X_1$	2.3g	2.3g
Transmissibility [%]	$\lvert T_r \rvert$	0.679	0.36

In both these cases the response is lower than for a conventional sub-frame while only adding 15% of the screen mass to the assembly. The additional weight of m_2 will require higher absorber stiffness and therefore a longer port. A sub-frame with the same mass (15%) will have a transmissibility of 8%, which is even higher than a screen with conventional isolators. Figures 5.13 to 5.15 show the response and transmissibility of an absorber with a feasible 20 mm static deflection.

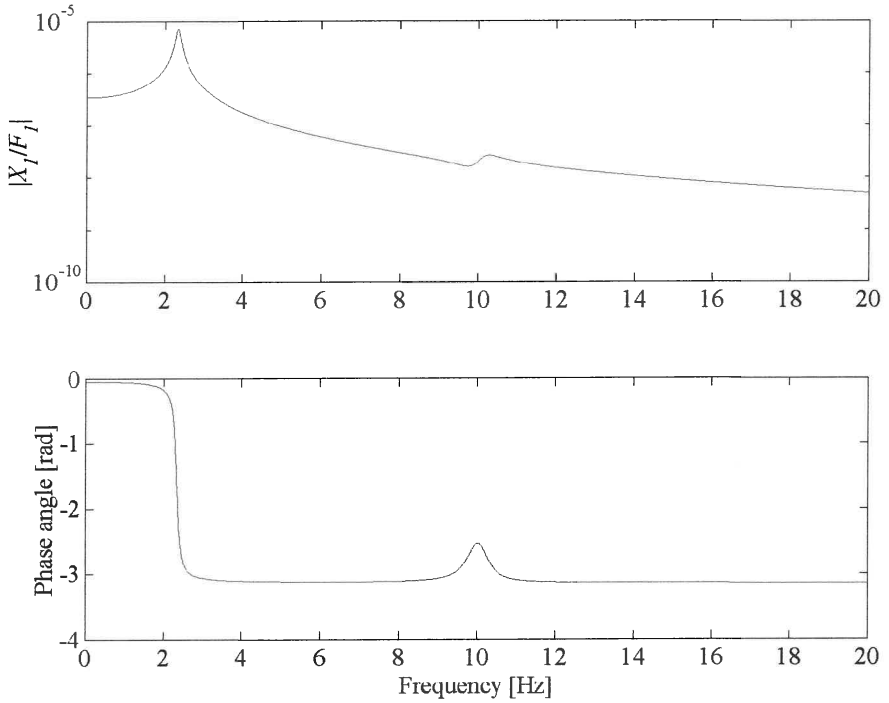

Figure 5.13 Response of the screen to the excitation force (x_2 = 20 mm)

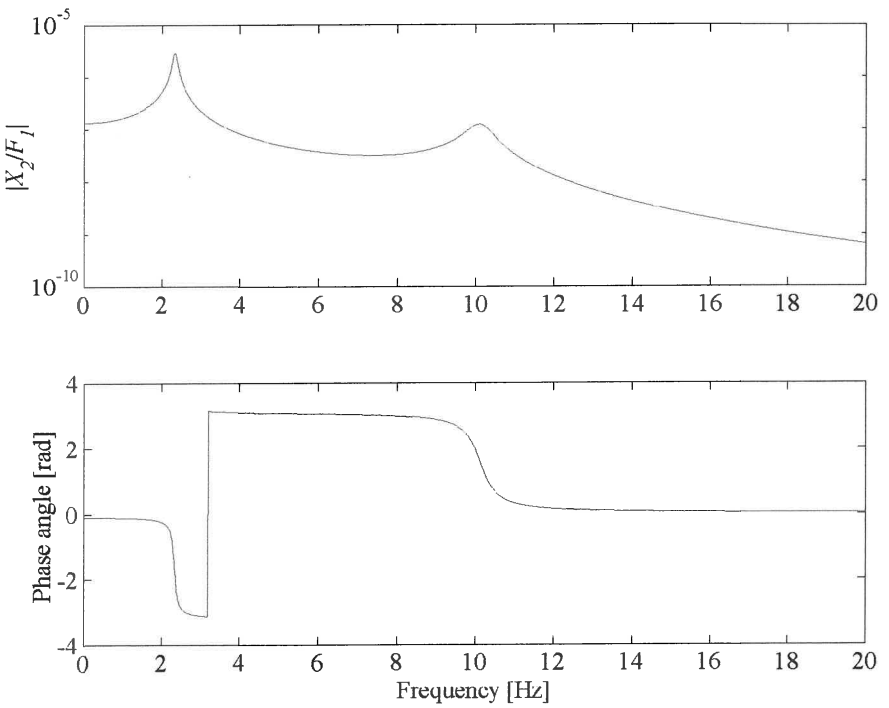

Figure 5.14 Response of the sub-frame to the excitation force (x_2 = 20 mm)

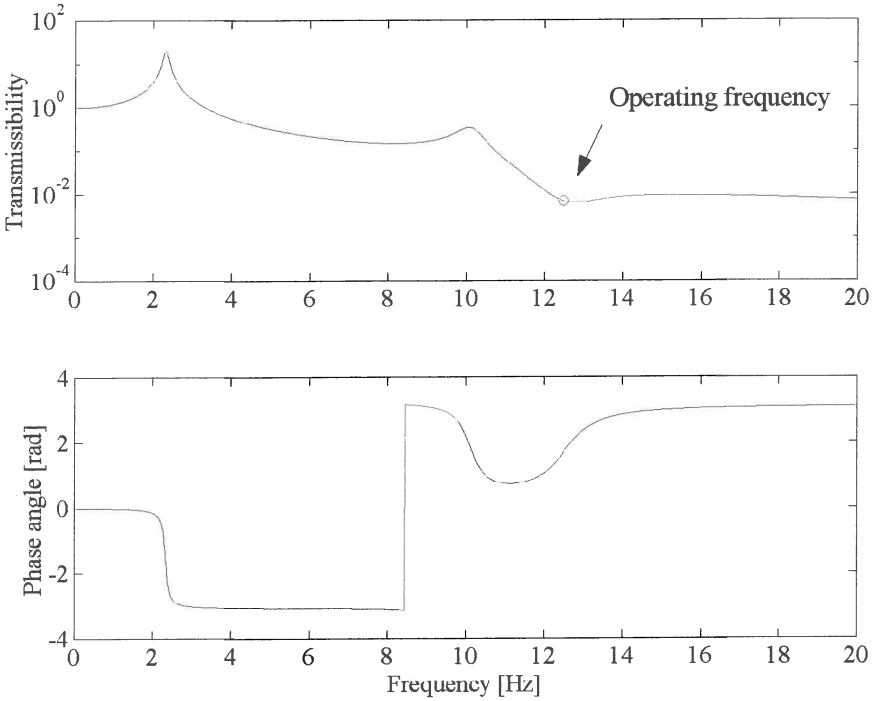

Figure 5.15 Transmissibility of the screen with an absorber fitted to the sub-frame (x_2 = 20 mm)

5.4 Conclusions

From the analysis presented in this chapter the following conclusions can be drawn:

- The single degree of freedom screen fitted with an absorber will offer the most benefit since good isolation can be achieved and there is no addition of mass to the system.
- The sub-frame fitted with an absorber will reduce the mass ratio for this type of design significantly. For applications where more isolation is needed than achievable with the single degree-of-freedom system this method is recommended.
- The damping of the absorber should be as low as possible.
- It is important that the absorber spring should be as soft as possible. It seems as if it will be difficult to design such a spring, but the anticipated problems can probably be overcome.
- The acceleration of the screen, which is the most important parameter affecting its operation, is not altered significantly using any of these methods.

Overall the liquid inertia vibration absorber has shown enough advantages over existing isolation methods for screens to warrant further development.

CHAPTER 6

Conclusions

Even though many industrial machines depend on vibration or oscillatory motion for their operation, such vibration may cause serious problems relating to their supporting structures, for instance fatigue damage. This study investigated how liquid inertia vibration absorbers can be used to attenuate the forces transmitted by vibrating screens.

In chapter 1 it was established that although vibration is essential to the proper working of a vibrating screen, the forces resulting from this operation are undesirable. Methods for the control of the vibration were presented. The current methods have certain drawbacks, which can be overcome with the use of vibration absorbers. Pendulum, hydraulic and liquid inertia absorbers were presented as possible solutions for screen isolation. The main advantage of these vibration absorbers is the excellent isolation that can be achieved with only a fraction of the weight increase associated with a sub-frame. The liquid inertia vibration eliminator (LIVE) absorber showed the most promise for this application because of its simple design and low maintenance requirements.

Next a detailed mathematical analysis of the LIVE system was presented. The effect of each variable on the system response was discussed. Arbitrary port inlet/outlet geometry was taken into account using Lagrange's equations. The viscous damping plays a very important role in the amount of isolation that can be achieved. The damping was analysed using CFD and methods for reduction were suggested. The lowest transmissibility resulted when the natural frequency was much smaller than the isolation frequency. This was found when the system mass is much larger than the absorber mass.

Chapter 3 showed how to design the LIVE absorber. Two methods for the design were discussed. The optimisation approach is recommended due to its ease of use. The numerous practical considerations for the design of these absorbers were highlighted. The possible absorber liquids were listed. Water was chosen as absorber liquid on cost and safety grounds. Considerable effort was made to predict the absorber stiffness. The summation of flat plate springs in series, representing the exact geometry, was found to be of adequate accuracy if compared to finite element results. The damping for the design was calculated and the addition of conical inlets/outlets reduced the amount of damping considerably. The viscous damping is a linear function of frequency. The inlets/outlets reduced the effective absorber mass and this reduction was compensated for by increasing the port length.

Chapter 4 discussed the methods used for the estimation of the spring stiffness and loss factor as well as the absorber transmissibility. The results showed that the stiffness was a function of time and that the spring rate could be described by an exponential decay function. The constant frequency excitation methods showed excellent agreement with sine sweep methods. The stiffness of the absorber was found to be a linear function of frequency. The absorber stiffness cannot be accurately predicted and in practice alteration to the port geometry will be

necessary after manufacture and testing of the spring. The loss factor for polyurethane was 0.12, which is considered to be low and did not vary appreciably with frequency. Elastomers with lower loss factors do exist although manufacturing these will be more difficult. Two springs were fitted to the absorber and both showed excellent transmissibility results. The softer spring had a transmissibility of 16% at 42 Hz, which was lower than the 55 Shore A as predicted. Softer springs and less damping can improve these results.

Chapter 5 presented and analysed two possible configurations showing how an absorber can be added to a screen. First the absorber was fitted to a screen and then to a sub-frame. The addition of a realistic absorber showed that the transmissibility could be reduced significantly. The absorber fitted directly to the screen showed the most promise since the addition of weight was negligible, while reducing the transmissibility with a factor of 7.2. Fitting the absorber to the sub-frame gave similar transmissibility results to that of a screen fitted with a sub-frame only, but the mass ratio was only 15%.

This study laid a sound mathematical base for the design of LIVE type vibration absorbers. Future work should include:

- The optimisation of the port geometry for the minimum amount of the flow damping. This should be done using CFD and an optimisation algorithm.
- A major design challenge remains the active control of the isolation frequency. Although some work has been done in this area, a cost-effective method hasn't been proposed yet.
- The bulk of any future work should be experimental testing of various absorber designs and isolation frequency control methods.
- An investigation of cost effective manufacturing of the absorber and specifically of the elastomeric spring should be undertaken.
- Alternative castable, low loss factor elastomers must be found.
- Physical configurations of absorbers in screen suspension systems must be investigated.
- A detailed cost comparison between conventional isolation systems and vibration absorbers must be made.